

J.-P. Boulanger

The Trident Pacific model. Part 1: simulating surface ocean currents with a linear model during the 1993–1998 TOPEX/POSEIDON period

Received: 28 May 1999 / Accepted: 18 May 2000

Abstract Zonal advection by long equatorial waves has been shown to be an important process in the evolution of sea surface temperature in the central Pacific on ENSO time scales. The present study aims at investigating how well an oceanic model whose dynamics are based on long equatorial waves can simulate the large-scale surface zonal current variability. Thus an ocean linear model which can be run with two or three layers is validated against several sets of observations in the Pacific ocean (TOPEX/POSEIDON sea level, TAO zonal currents, surface current climatology). The surface layer (mixed-layer) has a constant depth. Therefore the layer model is equivalent to considering a shear layer solution and either one or two baroclinic modes. It allows evaluation of the impact of adding a second baroclinic mode on the simulation of surface currents. This evaluation is done for different friction parametrizations: a weak linear Rayleigh friction (24 months^{-1}), a strong linear Rayleigh friction (6 months^{-1}), and a new parametrization using quadratic friction in the momentum equation only. It is shown in all simulations using various Rayleigh friction parametrizations that the addition of a second baroclinic mode always improves the simulation of both the sea level and the surface currents, especially in the central western Pacific. In that region, there is a reduction of the propagating long Rossby waves whose amplitude is much too large when only one baroclinic mode is used. Despite this reduction, the use of a weak friction (24 months^{-1}) always yields results which compare only poorly to observations confirming results from previous studies. The use of strong friction (6 months^{-1}) improves the model simulation, but surface current variability still remains too large. Finally, the use of

quadratic friction as proposed in the present study considerably improves the simulation of zonal currents and its comparison to all data sets. This result gives more confidence in the choice of such a simple model to further explore the role of zonal advection by long equatorial waves on ENSO time scales.

1 Introduction

Long equatorial wave theory (Moore and Philander 1977; Cane and Sarachik 1976, 1977, 1979; McCreary 1985) has been shown to explain a large part of the variance of the observed low-frequency tropical Pacific ocean sea level and surface current variability (Miller et al. 1988; Delcroix et al. 1991, 1994; Boulanger and Menkes 1995, 1999; Picaut and Delcroix 1995; Boulanger and Fu 1996). Moreover it has been considered as the dynamical foundation for various potential theories of the El Niño/Southern Oscillation (Schopf and Suarez 1988; Battisti 1988; Picaut et al. 1997). During the Tropical Ocean Global Atmosphere (TOGA) programme, ocean-atmosphere coupled models (e.g. Zebiak and Cane 1987) have been designed such that linear ocean dynamics are used to represent mainly equatorial Kelvin and long Rossby waves. In parallel, the efforts of the modelling scientific community since the 1980s have led to the development of general circulation models (GCMs) of the ocean and the atmosphere with more complex physics. Although these models offer a better representation of the physical processes on various temporal and spatial scales, simple models are still extremely useful to understand potential mechanisms and physical balances at work in the coupled system, which can then be investigated in more general complex models.

As examples, linear ocean models used for ENSO studies can either use only one baroclinic mode (Busalacchi and O'Brien 1981; Busalacchi et al. 1983), multiple baroclinic modes (Busalacchi and Cane 1985;

J.-P. Boulanger
Laboratoire d'Océanographie Dynamique et de Climatologie,
UMR CNRS/ORSTOM/UPMC,
Université Pierre et Marie Curie, Tour 26/Etage 4/Case100,
4 Place Jussieu, 75252 Paris, Cedex 05, France
E-mail: jpb@lodyc.jussieu.fr

McPhaden and Yu 1999), one baroclinic mode and a shear surface layer (Zebiak and Cane 1987) or multiple baroclinic modes and a shear surface layer (Chen et al. 1995; Dewitte 2000). Some of these models have been used for theoretical studies or for comparisons to observations and have mainly been evaluated using data such as tide-gauge measurements (Busalacchi and Cane 1985), climatological surface current data (Dewitte 2000), Tropical Atmosphere Ocean (TAO) Array (Hayes et al. 1991; McPhaden 1993) observations (Kessler and McPhaden 1995), or TOPEX/POSEIDON (T/P) sea level anomalies (McPhaden and Yu 1999). Most of these models share the use of a linear Rayleigh friction to represent the dissipation of long equatorial wave amplitudes along their propagation [with values often smaller than $(24 \text{ months})^{-1}$ for the first baroclinic mode; this will be considered in the following as a weak friction]. This choice of weak friction means that long equatorial waves are very little damped and can bounce back and forth at the Pacific boundaries. Various comparisons to sea level data (Picaut et al. 1993; Kessler and McPhaden 1995; Boullanger and Fu 1996; McPhaden and Yu 1999) have highlighted the importance of using friction values larger than $(12 \text{ months})^{-1}$ (referred to in the following as a strong friction) to properly reproduce sea level or dynamic height anomalies in the equatorial Pacific basin. To this day, very little attention has been given to the validation of surface currents simulated by such linear ocean models even though those currents play a key role in ENSO (Picaut et al. 1996) and on which simple coupled models of ENSO are based (Picaut et al. 1997).

The aim here is thus, first, to investigate the skill of such linear models in simulating surface currents when using the typical linear Rayleigh friction with one or two baroclinic modes, and, second, to explore how these can be satisfactorily simulated on ENSO time scales. Such an exploration is crucial if one wants to use such linear models to evaluate the role of zonal advection by long equatorial waves on ENSO as has been illustrated in data analysis (Picaut et al. 1996). To perform such an investigation, a linear ocean model similar to other linear ocean models is validated during the 1993–1998 period during which multiple basin-scale high-quality observations are available (e.g. ERS and TAO wind forcing, T/P sea level anomalies and TAO surface zonal currents).

Briefly, the oceanic dynamics is derived from a linear 3-1/2 layer model, with a constant surface layer (mixed-layer). Fluxes of mass and momentum are allowed between the first and second layers. As the surface layer has a constant depth, only two baroclinic modes exist in the model. Finally, the major parameters of this oceanic model are the number of subsurface layers (equivalent to the number of baroclinic modes; two subsurface layers are considered in the standard version), the density and thickness of each layer (determining in particular the phase speed and wind projection coefficient for each baroclinic mode), the parametrization of the flux of

momentum and mass between the first and second layers, and the parametrization and amplitude of the friction in each layer.

Section 2 presents the various data (TOPEX/POSEIDON sea level, zonal currents from the TAO Array, ERS + TAO surface wind stress data). Section 3 describes the model grids and equations. Section 4 discusses the comparison of the oceanic model dynamics to data and its simulated variability during the 1993–1998 period. Section 5 discusses the model sensitivity to major parameters. Finally, Sect. 6 discusses the results and gives some conclusions.

2 Data

TOPEX/POSEIDON sea level data

The TOPEX/POSEIDON sea level data used in the present study are provided by the Center of Space Research at the University of Texas. A detailed description of the data processing and error analysis can be found in Tapley et al. (1994). The sea level data gridded on a 1° longitude by 1° latitude regular grid for each cycle are averaged onto the model grid. Data are monthly averaged. We use the first 230 cycles for the period October 1992–December 1998. Sea level anomalies are computed relative to the January 1993–December 1996 period, which showed weak interannual variability (Boullanger and Menkes 1999). Only monthly means will be considered here.

TOGA-TAO zonal current data

One of the great achievements of the TOGA-TAO array is to provide long time series of current profiles at different locations along the equator (110°W , 140°W , 170°W , 165°E , 156°E and 147°E). At these sites in-situ currents are measured with six to seven vector averaging current meters (VACMs) and/or with the acoustic doppler current profiler (ADCP). Both kinds of measurements are highly correlated (McPhaden and McCarty 1992). Where both kinds of measurements were available, ADCP observations were preferred. All data at each mooring location were monthly averaged. Data were then processed in the following way. First, following the methods described in McPhaden and McCarthy (1992), missing data at a given level were either interpolated (when close upper and lower levels were available) or extrapolated (when only one level was available) through either bilinear or linear regression. A 1-2-1 filter is then applied in time at each mooring level.

The model surface currents are computed over 50 m (the thickness of the surface layer), however they actually represent the currents vertically averaged over the mixed-layer. Therefore the question arises as to what current observations should be considered to validate the model. First, it is a difficult task to compute the exact depth of the mixed-layer (especially as salinity measurements are not available at most of the mooring sites). Second, one could consider that the mean mixed-layer thickness is close to 30 m in the eastern and western Pacific basins while it is deeper in the central Pacific. In fact, averaging observed currents over 30 m in the eastern and western Pacific or over 70 m in the central Pacific as compared to considering only the near-surface currents would not strongly affect the model-data comparisons except in the eastern Pacific during cold phases when the core of the Equatorial UnderCurrent and the thermocline shallow significantly (i.e. the mixed-layer shallows as well). Therefore, considering the previous points and, for the sake of simplicity, all comparisons to TAO moorings will be performed using 10-m current data, except at 170°W where the ADCP was mounted on a subsurface mooring looking upward from about 270 m depth. At that location, the 30-m depth measurement is the shallowest measurement unaffected by

side-lobe reflections from the surface and is therefore chosen for comparisons.

ERS + TAO wind stress data

ERS-1 and ERS-2 wind data were provided by the Centre ERS d'Archivage et de Traitement located in the Institut Français de Recherche pour l'Exploitation de la Mer. The method used to convert the radar backscatter measured by the ERS-1 and ERS-2 scatterometers is described and validated in Bentamy et al. (1996). The original product is gridded on a 1° longitude by 1° latitude regular grid and is a weekly average wind stress field. A recent study (Menkes et al. 1998) has highlighted the weak amplitude of the ERS wind stress in comparison to TAO wind data, leading to the choice of using the ERS + TAO wind stress data set constructed by Menkes et al. (1998). Data are spatially (2° longitude \times 0.5° latitude) and temporally (5-day time step with six time steps per month) interpolated onto the model grid. ERS-1 data were used from May 1992 to May 1996 while ERS-2 data were used from June 1996 to December 1998. A climatology was computed over the period January 1993–December 1996. Wind stress interannual anomalies are computed relative to that period.

3 The oceanic model dynamics

The oceanic basin extends from 130°E to 80°W in longitude and from 20.25°S to 20.25°N in latitude. The grid resolution is 2° in longitude and 0.5° in latitude. The resolution is the same in each layer. The model spatial grid is displayed in Fig. 1.

The model dynamics is derived from a 3-1/2 layer linear model considering the following hypotheses: (1) the first layer (mixed-layer) has a constant depth; (2) the interface between the first and second layer is not a material surface i.e. there are fluxes of mass and momentum through the interface; and (3) the interface between the second and third layer (representative of the top of the thermocline) is considered as a material surface with no flux through the interface. Thus, the 3-1/2 layer model is equivalent to solving a shear-layer and two subsurface equations.

Introducing $(\mathbf{u}_1, \mathbf{v}_1)$ as the currents in the first layer, $(\mathbf{u}_2, \mathbf{v}_2)$ as the currents in the second layer, $(\mathbf{u}_s, \mathbf{v}_s)$ as the shear currents between the first and second layers, and (H_1, H_2) as the thickness of the first two layers:

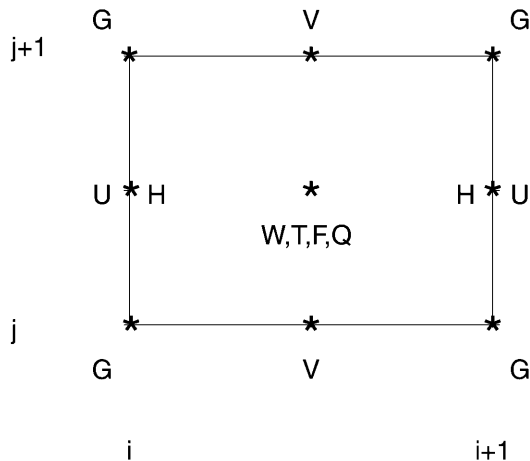


Fig. 1 Model discretization grid. U , V , W , H , T , F , G and Q respectively refer to the zonal current, meridional current, vertical current, sea level (or pressure), temperature, zonal forcing, meridional forcing and “mass” forcing

$$\begin{cases} \partial_t \mathbf{u}_s - \beta y \mathbf{v}_s = \frac{\tau_0^x}{\rho_0 H_1} - \frac{\tau_1^x}{\rho_0} \left(\frac{1}{H_1} + \frac{1}{H_2} \right) \\ \quad + K_H \Delta_H \mathbf{u}_s + \text{Fric}(\mathbf{u}_1) - \text{Fric}(\mathbf{u}_2) \\ \partial_t \mathbf{v}_s + \beta y \mathbf{u}_s = \frac{\tau_0^y}{\rho_0 H_1} - \frac{\tau_1^y}{\rho_0} \left(\frac{1}{H_1} + \frac{1}{H_2} \right) \\ \quad + K_H \Delta_H \mathbf{v}_s + \text{Fric}(\mathbf{v}_1) - \text{Fric}(\mathbf{v}_2) \\ w_s = H_1 (\partial_x \mathbf{u}_s + \partial_y \mathbf{v}_s) \end{cases} \quad (1)$$

where τ_0^x and τ_0^y are the zonal and meridional wind stresses and τ_1/ρ_0 is taken as a vertical diffusion term at the base of the mixed-layer i.e. $\tau_1/\rho_0 = (K \partial_z \bar{\mathbf{u}})_{z=H_1} = K \bar{\mathbf{u}}_s / H_1 = K_u \bar{\mathbf{u}}_s$. From the previous equations, near the equator, the upwelling velocity is roughly proportional to $(H_1 H_2) / (K_u (H_1 + H_2))$. The value of K_u was chosen in each experiment (control and sensitivity) for the model maximum mean upwelling velocity at the equator to be close to 2.5 m/day which is close to observed values (e.g. Bryden and Brady 1985; Halpern 1987). Actually, this term represents the transfer of momentum from the surface to the base of the mixing layer i.e. it includes the effect of vertical mixing and of entrainment/detrainment related to the vertical displacement of the mixed-layer, a mechanism not explicitly simulated by the model. For the sake of simplicity this value is constant in time and space. The dissipation is the sum of a horizontal Laplacian diffusion and a friction term which will be discussed later. The horizontal diffusion coefficient is chosen as $2000 \text{ m}^2 \cdot \text{s}^{-1}$ except near the western boundaries where this value becomes $40\,000 \text{ m}^2 \cdot \text{s}^{-1}$. It also slowly increases from 2000 in the 10°N – 10°S band up to 40 000 at the northern and southern boundaries (20°). The choice of such large values near the western boundary and near the model meridional boundaries is motivated by the need to avoid large values of the vertical velocity computed at the western and meridional boundaries. Indeed, a large vertical velocity at the western boundary otherwise affects the baroclinic solution computed in the subsurface equations. Moreover, near the northern and southern model boundaries, the large diffusion coefficient allows one to reduce the forcing of the anti-Kelvin waves in the subsurface equations.

Considering the following points: (1) $w_1 = w_s + H_1 (\partial_x \mathbf{u}_2 + \partial_y \mathbf{v}_2)$, (2) the subsurface dynamics at low frequency is mainly dominated by long Kelvin and Rossby waves (i.e. the system can be reduced using the long wave approximation), the subsurface layer equations ($k = 2, 3$) are:

$$\begin{cases} \partial_t \mathbf{u}_k - \beta y \mathbf{v}_k + \partial_x (p_k / \rho_0) = \frac{\tau_1^x}{\rho_0 H_k} \delta_{2k} + \text{Fric}(\mathbf{u}_k) = F_k \\ + \beta y \mathbf{u}_k + \partial_y (p_k / \rho_0) = \frac{\tau_1^y}{\rho_0 H_k} \delta_{2k} + \text{Fric}(\mathbf{v}_k) = G_k \\ \partial_t h_k + H'_k (\partial_x \mathbf{u}_k + \partial_y \mathbf{v}_k) = -w_s \delta_{2k} + \text{Fric}(h_k) = Q_k \end{cases} \quad (2)$$

where \mathbf{u}_k , \mathbf{v}_k , w_k , h_k , H_k , p_k , τ_k^x , τ_k^y respectively represent the zonal, meridional, and vertical current components, the anomalous layer thickness, the mean thickness, the anomalous layer pressure, and the zonal and meridional stress components between the layers k and $k + 1$. Moreover $H'_2 = H_1 + H_2$, $H'_3 = H_3$, and $\delta_{ij} = 1$ if $i = j$ and $\delta_{ij} = 0$ otherwise. Frictional terms are also considered, and their analytical form will be discussed later. Finally, the surface currents are the sum of the shear currents and of the second layer currents. The sea level anomalies are $\eta = \sum_{n=2}^3 h_n (\rho_4 - \rho_n) / \rho_0 = P_2 / \rho_0$.

The model equations correspond to a layer model. However, in order to solve the equations with a large time step (5 days), the model subsurface layer equations are at each time step decomposed into their equivalent baroclinic mode equations (see Appendix A) solved using a numerical scheme similar to Cane and Patton (1984).

The temporal discretization is a leapfrog scheme, and an Asselin filter (Asselin 1972) is used to remove temporal instability. When integrating from time step $n - 1$ to $n + 1$, the stress terms are those at time step n , while all dissipation and friction terms are explicit and computed from the solution at time step $n - 1$.

Frictional terms

The frictional terms (applied to the layer equations) can have two forms:

– the linear Rayleigh formulation

$$\begin{cases} \text{Fric}(\mathbf{u}_k) = -r_k^u \mathbf{u}_k \\ \text{Fric}(\mathbf{v}_k) = -r_k^v \mathbf{v}_k \\ \text{Fric}(h_k) = -r_k^h h_k \end{cases}$$

– a quadratic friction on the momentum, a linear friction on the layer thickness

$$\begin{cases} \text{Fric}(\mathbf{u}_k) = -r_k^u \mathbf{u}_k |\mathbf{u}_k| \\ \text{Fric}(\mathbf{v}_k) = -r_k^v \mathbf{v}_k |\mathbf{v}_k| \\ \text{Fric}(h_k) = -r_k^h h_k \end{cases}$$

The linear Rayleigh friction has been currently used in various similar models (e.g. Zebiak and Cane 1984; Battisti 1988; Chen et al. 1995; Dewitte 2000). Following McCreary (1981), this formulation has a theoretical basis only if the vertical diffusion coefficient profile is inversely proportional to the square of the Brünt-Vaisala frequency.

The use of a quadratic friction is to mimic in a crude way the role of non-linear dissipative processes in the momentum equations due to non-linear processes not resolved by the model physics. Focusing on low-frequency zonal currents, the non-linear term of the full momentum equations ($-\mathbf{u}\partial_x \mathbf{u}$), would decelerate eastward currents when $\partial_x \mathbf{u} > 0$ and westward currents when $\partial_x \mathbf{u} < 0$. Therefore around the equator, from the position of the maximum of the SEC westward to the convergence zone near the dateline (Picaut et al. 1996), the surface westward currents would be decelerated by this non-linear process. However in the region of the NECC, surface currents would instead be accelerated by non-linear processes, as well as in the eastern Pacific where the EUC surfaces. Therefore in these two regions the quadratic friction parametrization will not improve the surface current simulations while in the central and western Pacific, it will help in strongly damping the propagation of long Rossby waves whose amplitudes are often overestimated in linear ocean models. Whether such an effect can also be achieved using linear Rayleigh friction with more than one baroclinic mode

will be discussed. Finally, one must be conscious of the fact that, as stated in the case of Rayleigh friction (Blumenthal and Cane 1989), such a parametrization of friction is artificial as well.

As far as dimensions are concerned, the quadratic friction coefficient can be considered as a Rayleigh coefficient divided by a constant current amplitude. If we consider a constant current amplitude of order 10 cm/s (close to the mean value of the TAO 10-m zonal currents in the central and eastern Pacific), then the quadratic friction acts as a Rayleigh friction with an equivalent time scale proportional to $\mathbf{u}/0.1$ (\mathbf{u} being in m/s). Thus, it appears that when the surface current is larger than 10 cm/s the equivalent Rayleigh friction increases while when the surface current is smaller than 10 cm/s the equivalent Rayleigh friction decreases. Such a quadratic friction is therefore equivalent to a Rayleigh friction with a spatial and temporal variability. Indeed it acts more strongly in the central and eastern Pacific than in the western Pacific. As well, it acts more strongly during La Niña years (when the horizontal structures of currents are strengthened) than during El Niño years (when the total currents are weak and show weaker horizontal gradients). Considering the quadratic friction amplitude (Table 1), the equivalent Rayleigh friction for a surface current amplitude of 10 cm/s is equal to $(3.5 \text{ months})^{-1}$.

Model limitations

Even if the use of the quadratic friction helps in simulating the amplitude and variability of surface currents (as shown in the following section), the model does not have all the physics required to properly simulate surface currents. First, the model does not have a variable mixed-layer which would affect how the wind projects itself into the ocean. Second, as the model is linear it does not realistically simulate the springtime reversal of the South Equatorial Current. The dynamics of that reversal rely on a nonlinearity of the mean state as described in Yu et al. (1997) and Yu and McPhaden (1999). As will be shown later, it simulates a seasonal cycle with a springtime reversal, but the surface mean flow in the model is too strong to the west as a result of the linear dynamics. Second, the model does not simulate tropical instability waves and eddies which have been shown to be important in properly simulating both zonal and meridional advection (Wang and McPhaden 1999; Vialard et al. 2000). However the Trident model is designed to study the

Table 1 Model parameters for different sensitivity experiments

	M2FQ	M1FQ	M2WF	M1WF	M2SF	M1SF
H_1 (m)	50	50	50	50	50	50
H_2 (m)	25	25	80	80	55	55
H_3 (m)	174	–	302	–	244	–
$\rho_3 - \rho_2$ ($\text{kg} \cdot \text{m}^{-3}$)	3.73	10.87	2.15	6.27	2.67	7.76
$\rho_4 - \rho_3$ ($\text{kg} \cdot \text{m}^{-3}$)	2.83	–	1.62	–	2.02	–
c_1 (m/s)	2.80	2.80	2.80	2.80	2.80	2.80
c_2 (m/s)	1.27	–	1.27	–	1.28	–
$\gamma_1(H_1 + H_2)$	150	75	260	130	210	105
$\gamma_2(H_1 + H_2)$	150	–	260	–	210	–
$\text{Fric}_1(\mathbf{u}, \mathbf{v})$	2.85 ^a	2.85 ^a	1/24	1/24	1/6	1/6
$\text{Fric}_1(h)$	1/9	1/9	1/24	1/24	1/6	1/6
$\text{Fric}_2(\mathbf{u}, \mathbf{v})$	2.85 ^a	–	1/24	–	1/6	–
$\text{Fric}_2(h)$	1/9	–	1/24	–	1/6	–
K_u (m/s)	$4.7 \cdot 10^{-5}$	$4.7 \cdot 10^{-5}$	$1.6 \cdot 10^{-4}$	$1.6 \cdot 10^{-4}$	$1.1 \cdot 10^{-4}$	$1.1 \cdot 10^{-4}$

^a Unit is in $\text{months}^{-1} \cdot \text{m}^{-1} \cdot \text{s}$. H_1 is the model surface layer (mixed-layer) thickness, H_2 is the thickness of the second layer, H_3 is the thickness of the third layer when it applies. $\rho_3 - \rho_2$ is the density difference between the second layer and the third layer (M2FQ, M2WF, M2SF) or the deep layer at rest (M1FQ, M1WF, M1SF), $\rho_4 - \rho_3$ is the density difference between the third layer and the deep layer at rest in the experiments (M2FQ, M2WF, M2SF). c_1 is the phase speed of the first baroclinic phase speed. c_2 is the phase speed of the second baroclinic phase speed when it applies. $\gamma_1(H_1 + H_2)$ and $\gamma_2(H_1 + H_2)$ represent the wind projection coefficients respectively for the first and second vertical modes. $\text{Fric}_{1,2}(\mathbf{u}, \mathbf{v})$ is the friction coefficient applied to the momentum equations respectively for the first and second subsurface layers when it applies. $\text{Fric}_{1,2}(h)$ is the linear Rayleigh friction coefficient applied to the thickness layer equation respectively for the first and second subsurface layers when it applies. All friction units are in $(\text{months})^{-1}$ except when stated otherwise (M2FQ, M1FQ). K_u is a coefficient of vertical transfer of momentum between the surface layer and the first subsurface layer

role of long equatorial waves in ENSO events. As a consequence, and keeping in mind the limitations cited above, it remains an interesting tool to investigate such a role.

Choice of the control run parameters (M2FQ)

The model parameters used in the control run (M2FQ) are summarized in Table 1. In order to compare to other studies (Dewitte 2000), the wind projection coefficients have been chosen such that an equal wind energy is projected onto each baroclinic mode. This is typical of the central Pacific vertical stratification (Dewitte 2000). Then the choice of the layer depths and of the density differences between the layers have been made for the baroclinic phase speeds to have reasonable values representative of the equatorial Pacific (Table 1). It is worth pointing out that the model simulations are not really sensitive to these parameters values in the range 2.2–3 m/s for the first mode and 1–1.5 m/s for the second mode. Finally, as stated earlier, the value of K_u has been chosen for the mean equatorial upwelling to reach a maximum value of 2.5 m/day. The friction parameters have been evaluated for the model to reproduce the amplitude of the sea level and surface currents. This will be discussed in Sect. 5. As shown later, for such a choice of parameters the model reproduces fairly well the sea level and zonal current observed variability.

4 Evaluation of the ocean model dynamics during the 1993–1998 period

The control experiment (May 1992–December 1998) is preceded by a 5-year spin-up using the 1993–1996 wind stress climatology. Model outputs are monthly averaged. The model climatology was computed over the period January 1993–December 1996. Interannual anomalies are computed relative to that period.

Sea-level variability

The mean topography of the simulated sea level (Fig. 2a) displays the major observed features. On a seasonal time scale, the model compares fairly well to the seasonal cycle computed from T/P data in the central Pacific (170°E–140°W) around the equator (Fig. 2d). However it poorly simulates the sea level seasonal cycle in the eastern Pacific (correlation lower than 0.2 at 110°W) and north of 5°N where the model simulates unrealistic amplitudes (Figs. 2b, e). In the eastern Pacific, this pattern may be due to at least two reasons: 1) the observed sea level variability (Fig. 2c) is rather weak (between 1 and 2 cm) inducing a rather low signal-to-noise ratio; 2) the model is unable to properly simulate the springtime reversal of the zonal current which in the real ocean is due to nonlinear processes (Yu et al. 1997; Yu and McPhaden 1999). This can affect the sea level variability in a region of weak variability. The simulated pattern north of 5°N is an overestimated response to the wind stress curl in that region actually very sensitive to the wind stress product (see Fig. 11 of Busalacchi et al. 1990). Although, the ERS + TAO wind product is likely one of the best wind products that can be used for a Pacific Ocean simulation in the 5°N–5°S band, the combined wind data set can experience, at the poleward

boundaries of the TAO array (8°N–8°S), a meridional gradient (transition from ERS + TAO winds to ERS winds only) which would affect the wind stress curl. Between 5°N and 10°N, the region over which meridional displacement of the ITCZ occurs, such a wind stress curl might indeed generate a significant spurious signal in sea level. Interannual anomalies (Fig. 2f) display patterns of variability similar to the ones observed in T/P data (Fig. 2g) although the model has a larger amplitude in the western Pacific. The correlation (Fig. 2h) is larger than 0.7 over the entire 5°N–5°S band with maxima over 0.9 in the western Pacific and in the central Pacific. The mean correlation reached 0.88 in the 5°N–5°S band with a mean rms difference of 4.1 cm (Fig. 2i). In summary, the model exhibits reasonable skill in simulating sea level variability in the equatorial wave guide.

Surface zonal current variability

The model surface zonal currents are first compared to the TAO zonal currents (Fig. 3). It is found (see Table 2) that the model represents the observed zonal current amplitude over the entire basin fairly well, although correlations are better in the western-central Pacific than in the eastern Pacific. At 110°W, in particular, the model-data comparison is 0.51, because the actual springtime reversal is due to nonlinear processes (Yu et al. 1997; Yu and McPhaden 1999) that the linear model cannot reproduce.

The model mean state and seasonal cycle variability are then compared to the Reverdin et al. (1994) climatology. As can be seen in Fig. 4a, b, the model does not reproduce the amplitude of the NECC, and the northern branch of the SEC extends too far poleward. In addition, the model captures the basic mean state computed over another period (1987–1992) using surface drifters. The northern branch is stronger than the southern branch. An equatorial minimum is found east of 130°W. The seasonal cycle variability for the data (Fig. 4c, d) displays a larger variability along the equator than in the model (Fig. 4c) although the observed patterns have a spatial extension on the same order of the zonal resolution of the data grid (5°). On average, both model and data have variability on the order of 15 to 25 cm/s, and both display a coherent pattern of larger variability north of 8°N. In agreement with our previous results, it appears that the model does not simulate the larger equatorial variability observed in the eastern Pacific (130°W–90°W). Interannual anomalies (Fig. 4e) display larger variability near the dateline (region of large interannual wind anomalies) and in the central-eastern Pacific near 5°N in the region of displacement of the ITCZ.

Surface meridional current variability

The model surface meridional currents are compared to the Reverdin et al. (1994) climatology. Although the

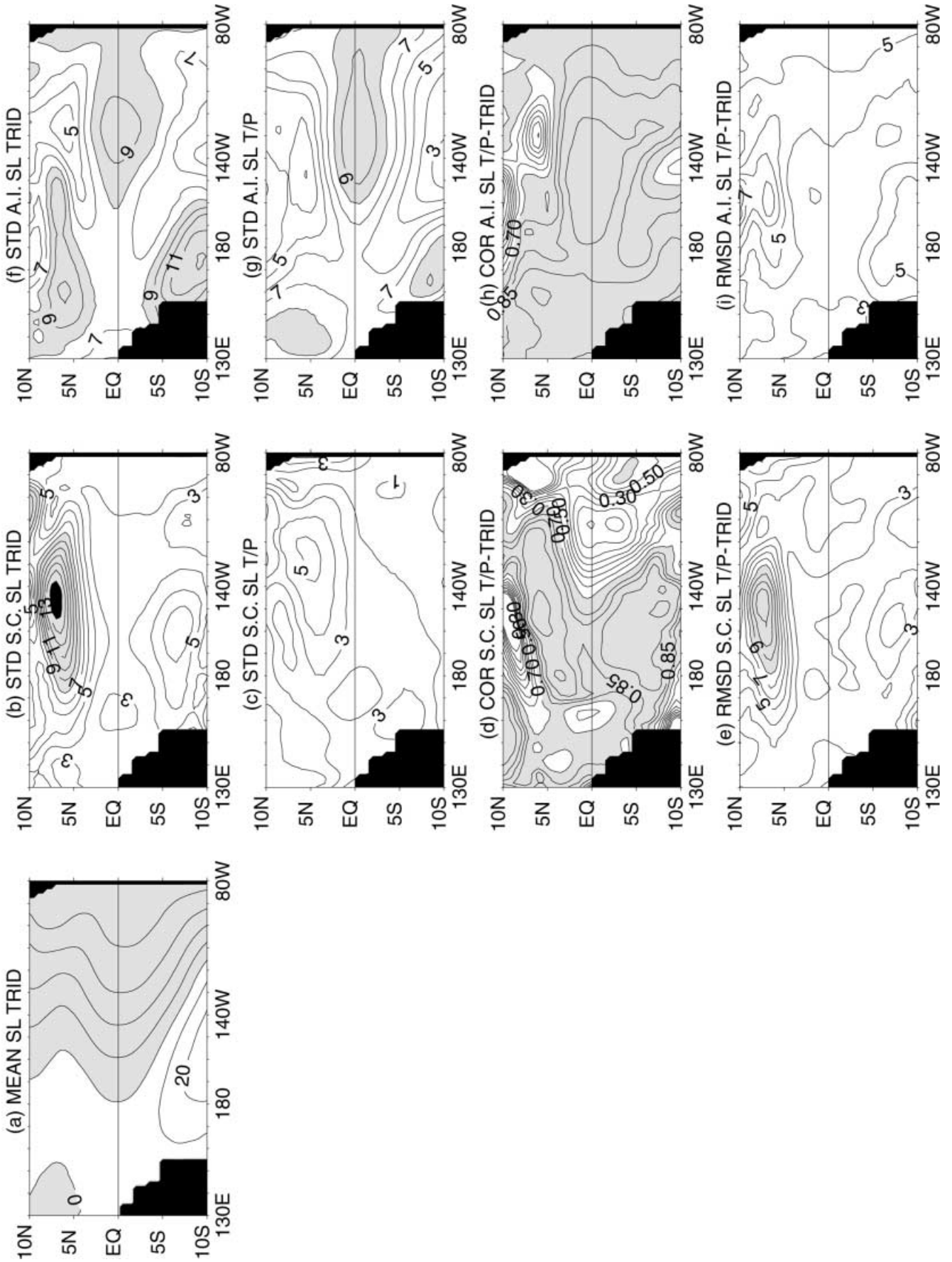


Fig. 2 **a** Model sea level mean state (contour intervals are every 10 cm; negative values are shaded); **b** model climatological variability (contour intervals are every 1 cm; values larger than 8 cm are shaded); **c** same as **b** but for *T/P* data; **d** map of correlation between *T/P* and simulated sea level climatologies (contour intervals are every 0.1 from 0. to 0.8, and every 0.05 from 0.80 to 0.95; values higher than 0.7 are shaded); **e** map of rms difference between *T/P* and simulated sea level climatologies (contours are every 1 cm; values higher than 8 cm are shaded); **f** same as **b** but for interannual anomalies; **g** same as **c** but for interannual anomalies; **h** same as **d** but for interannual anomalies; **i** same as **e** but for interannual anomalies

model (Fig. 5a) captures the average mean flows north and south of the equator (Fig. 5b), the model underestimates some patterns of mean meridional currents. This is also found when comparing the seasonal cycle variability (Fig. 5c, d). The observed large amplitudes might be the residual signatures of instability waves which near the equator strongly affects the meridional currents and

Table 2 Model comparisons with TAO surface zonal currents

TAO mooring	147°E	156°E	165°E	170°W	140°W	110°W
Correlation	0.80	0.81	0.88	0.77	0.62	0.51
Std TAO (cm/s)	27.6	22.0	35.1	33.8	32.7	33.5
Std Trident (cm/s)	28.1	24.9	30.8	32.0	28.6	21.2
Rms difference (cm/s)	17.7	14.8	16.7	22.4	27.0	29.1

which are not simulated by the model. Interannual anomalies have a larger variability in the western Pacific where the interannual wind anomalies are located.

Vertical current variability

The mean vertical current (Fig. 6a) displays an upwelling along the equator in the central Pacific displaced slightly southward in the eastern Pacific. The maximum amplitude reaches 3 m/day along the equator in agree-

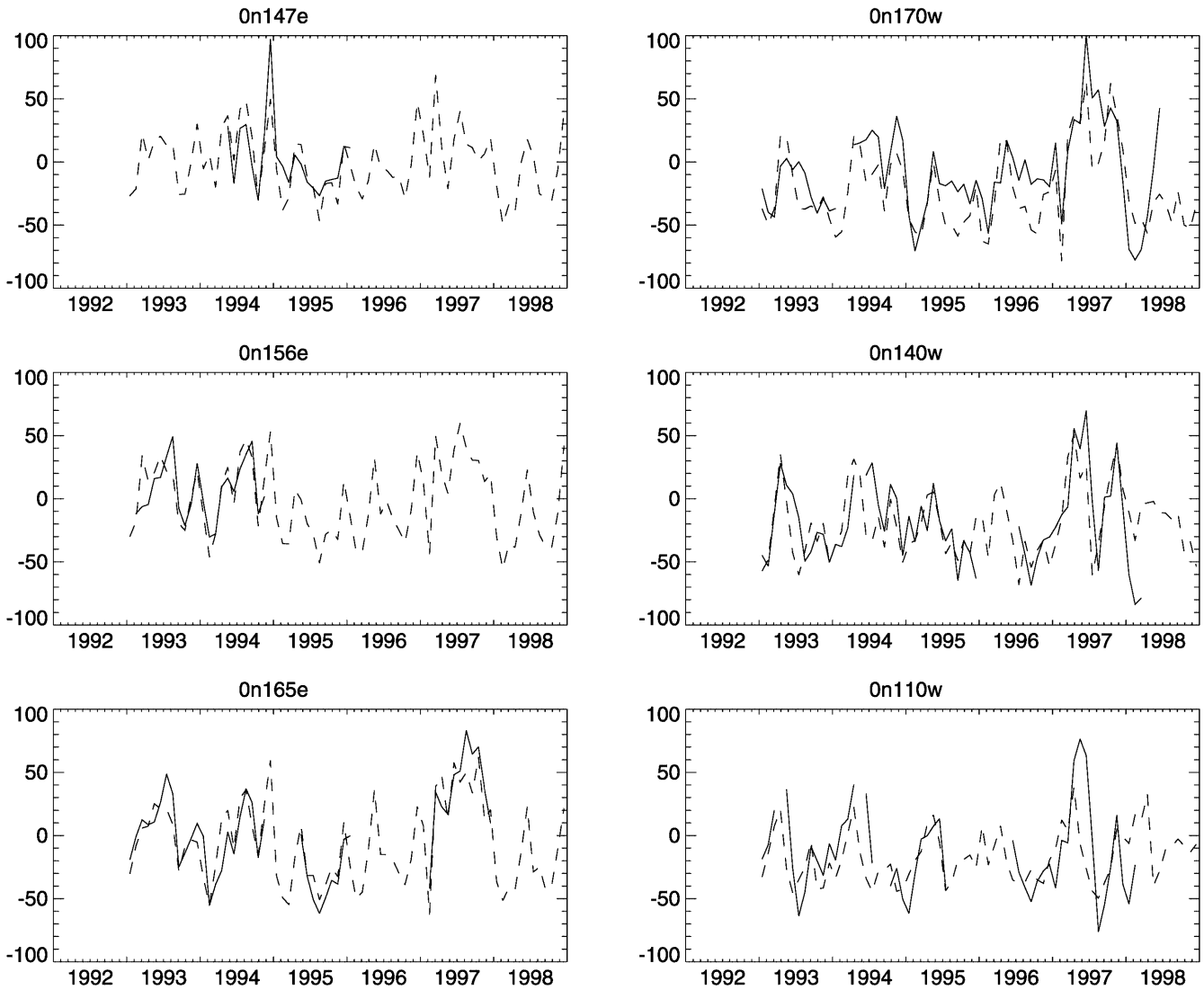


Fig. 3a-f Time series at **a** 147°E, **b** 156°E, **c** 165°E, **d** 170°W, **e** 140°W and **f** 110°W of TAO zonal current data (solid line) and simulated zonal currents (dashed line). Statistical comparisons are summarized in Table 2

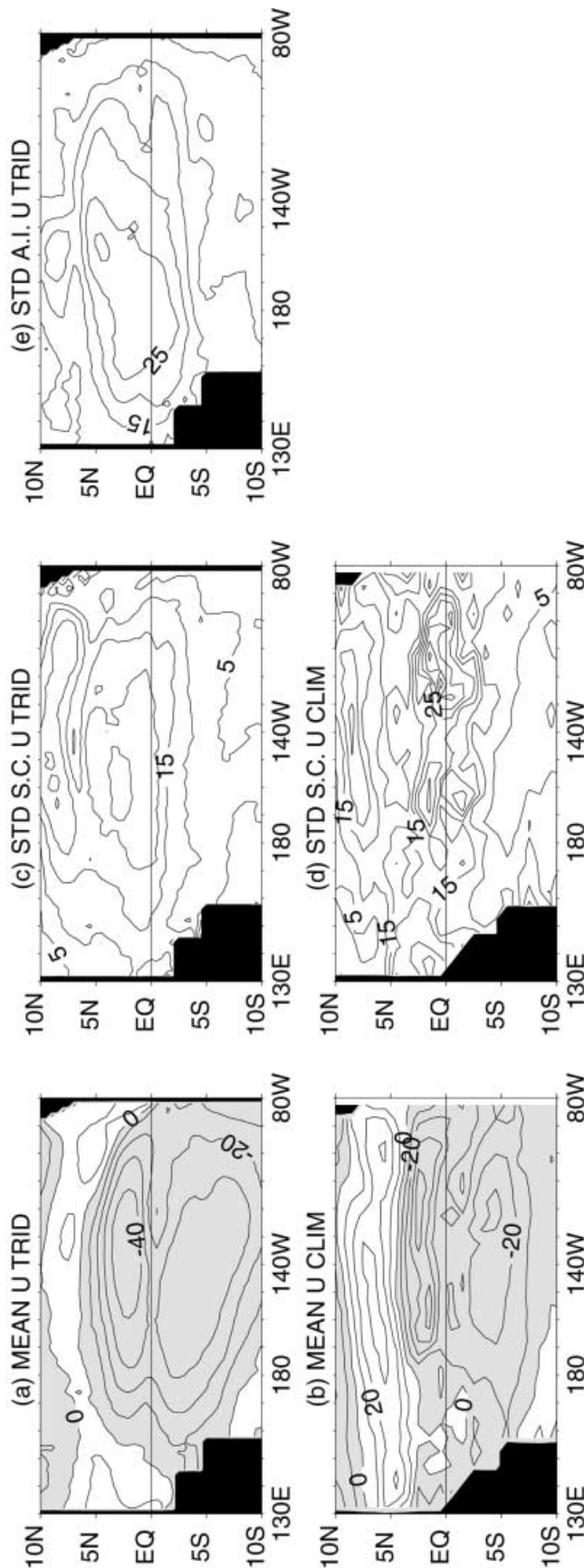


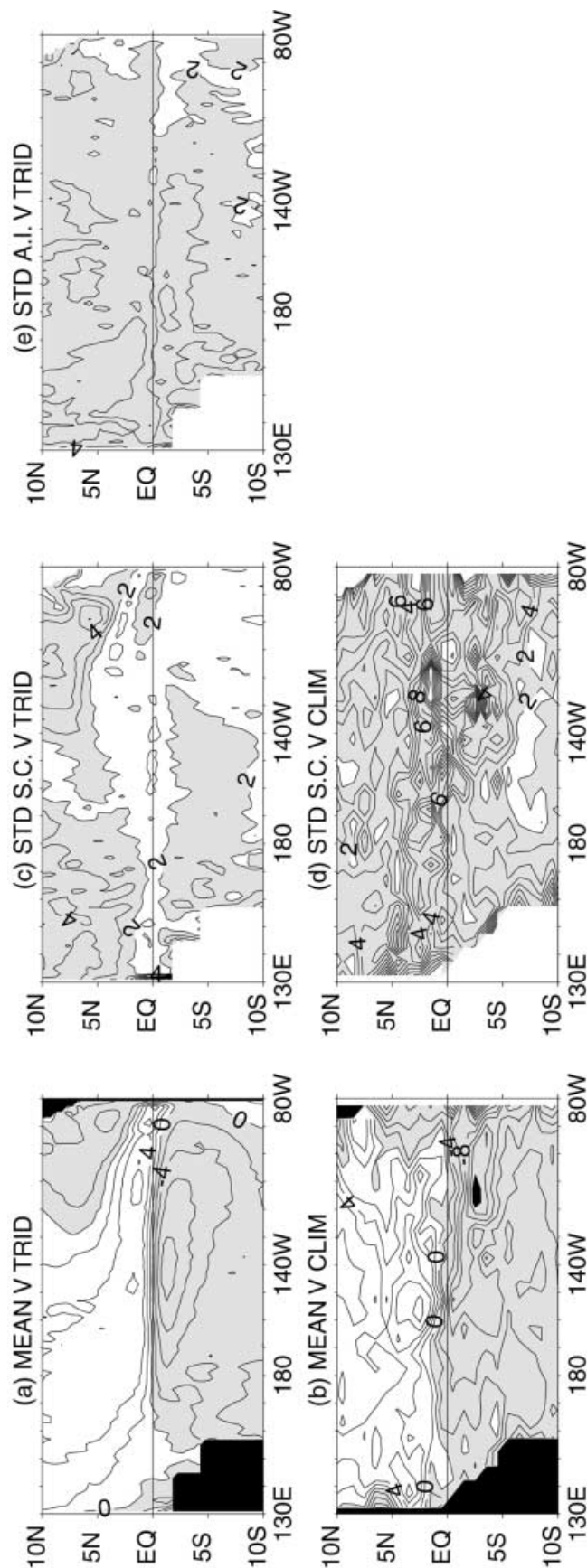
Fig. 4a–e Longitude–latitude maps (130°E–80°W/10°S–10°N) of: the mean surface zonal current from **a** the model and **b** the Reverdin et al. (1994) observations (contour intervals every 10 cm/s, negative values are shaded); the seasonal variability from **c** the model and **d** the Reverdin et al. (1994) observations (contour intervals every 5 cm/s); **e** the simulated interannual variability (contour intervals every 5 cm/s)

ment with various observations (Bryden and Brady 1985; Halpern 1987) and is also similar to the value found in an OGCM forced by the same winds (C. Menkes personal communication). Further east, the signal decreases as the maximum upwelling amplitude is actually displaced southward (Cromwell 1953). Westward, the equatorial upwelling also decreases until 142°E where the model coastlines get close to the equator. On seasonal and interannual time scales (Fig. 6b, c), the patterns of variability are rather noisy. During a seasonal cycle, along the equator (Fig. 7c, d), the model simulates a maximum upwelling velocity of 3 m/s (Fig. 7c) around 140°W. The minimum in the upwelling velocity happens when the trade winds weaken seasonally and when the springtime reversal of the zonal current is simulated (Fig. 7a).

5 Model sensitivity in simulating sea level and surface zonal currents

The main model parameters are: (1) the friction formulation and amplitude, (2) the number of baroclinic modes, (3) the layer parameters (layer density and thickness equivalent to the baroclinic phase speed and wind projection coefficient), and (4) the amplitude of fluxes of momentum and mass between the first and second layers (depending on Ku). First, for each simulation, the following model parameters (Ku , density and thickness layers) are adjusted: (1) for the mean upwelling velocity to reach 2.5 m/day near 140°W as in the control run; (2) for the sea level variability to reach similar amplitudes as T/P data in the eastern Pacific; and (3) for the mode phase speeds to be close to 2.8 m/s and 1.3 m/s. All experiment parameters are given in Table 1. Thus, only the model sensitivity to the friction parametrization and to the addition of a second baroclinic mode will be explored in the following.

First, we consider the 3-layer model (i.e. with two baroclinic modes) such that the wind projection coefficients for the two modes are equal. Three experiments are performed using respectively a (24 months)⁻¹ Rayleigh friction (M2WF), a (6 months)⁻¹ Rayleigh friction (M2SF) and a quadratic friction (M2QF). The same three experiments will then be performed with one baroclinic mode only (i.e. only two layers), and the respective simulations known as M1WF, M1SF and M1QF. These various simulations will be compared in terms of the sea level interannual variability (Fig. 8a–f), the mean zonal surface current (Fig. 8g–l), the zonal current climatological variability (Fig. 9a–f) and the zonal current interannual variability (Fig. 9g–l).



◀
Fig. 5a–e Same as Fig. 4 but for meridional currents. In **a, b**, contour intervals are every 2 cm/s, and negative values are *shaded*. In **c–e**, contour intervals are every 1 cm/s, and values higher than 2 cm/s are *shaded*

Sea level interannual variability (Fig. 8a–f)

It appears clear that all simulations using two baroclinic modes simulate more accurately the equatorially-trapped pattern of variability associated with the 1997–1998 event observed in *T/P* data (Fig. 2g). In addition, all simulations using a linear Rayleigh friction significantly overestimate the sea level variability in the north-western Pacific, mainly due to the propagation of long equatorial Rossby waves whose signatures will be observed in the following in the surface zonal current variability.

Mean zonal currents (Fig. 8g–l)

All simulations using linear Rayleigh friction simulate a very large amplitude for the northern branch of the SEC (larger than 80 cm/s), clearly in disagreement with observations (Fig. 4b). Only the use of quadratic friction allows one to simulate a reasonable amplitude. On average, there is no clear evidence that adding a second baroclinic mode improves the model mean state. The major difference between weak and strong Rayleigh friction is observed in the central and western Pacific, regions where Rossby waves explain a large part of the model variance. Indeed, as Rossby waves slowly propagate from east to west, their amplitude is strongly affected by the amplitude and formulation of the friction by the time they reach the central and western Pacific.

Zonal current climatological variability (Fig. 9a–f)

It is evident that the choice of two baroclinic modes affects significantly the zonal current amplitude in the central and western Pacific, and that this represents an improvement. Similarly, the use of a strong friction improves the simulated amplitude. However, the surface current variability remains much larger than the climatological variability (Fig. 4d). Only the use of a quadratic friction simulates reasonable amplitudes. It is worth noting that all the simulations display a minimum of variability in the eastern Pacific to the west of 110°W in disagreement with observations.

Zonal current interannual variability (Fig. 9g–l)

All simulations using linear Rayleigh friction display a pattern of large variability near 8°N. This could be the result of the wind stress curl of the ERS + TAO

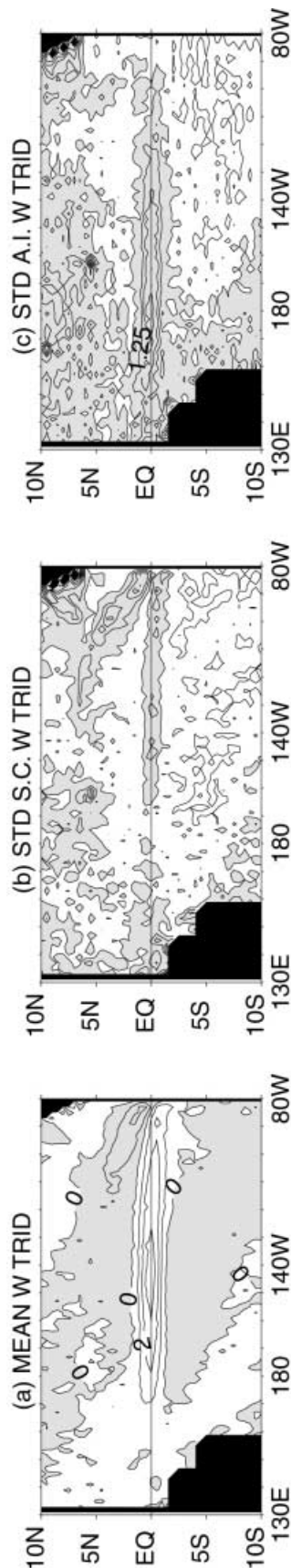


Fig. 6 **a** Mean vertical current at 50 m (contour intervals every 1 m/day, negative values are *shaded*), **b** the seasonal and **c** interannual variability of vertical currents (contours are every 0.25 m/day; in **b**, values larger than 0.5 m/day are *shaded*, and in **c**, values larger than 0.75 m/day are *shaded*)

wind product as discussed earlier. More interestingly, all simulations using linear Rayleigh friction display a larger variability along the equator near the dateline (by 5–10 cm/s) when two baroclinic modes are considered. This result is certainly related to the amplitude of the Kelvin waves which will reach the central Pacific after Rossby wave reflection at the western boundary. Indeed, as the second mode propagates more slowly than the first one, the Kelvin wave amplitude reaching the dateline coming from the reflection is more affected by friction. Thus the total Kelvin wave amplitude reaching the dateline in the two baroclinic mode case is weaker than in the one baroclinic mode case. Thus, as these Kelvin waves have equatorial zonal currents which sign is opposite to the impinging Rossby waves, the low-frequency Rossby wave amplitude wind-forced near the dateline is less counteracted by Kelvin wave reflection in the two baroclinic mode case. The total zonal current amplitude is therefore larger explaining the larger variability observed near the dateline.

Finally, regardless of whether one or two baroclinic modes are considered, all simulations with linear Rayleigh friction overestimate the surface current variability when compared to the model simulations using quadratic friction similar to the control run shown in Sect. 4 to reproduce the TAO data amplitudes fairly well.

6 Discussion and conclusions

The aim of the present paper was to improve the simulation of surface zonal currents in the Pacific Ocean using a linear model based on long equatorial wave dynamics. Indeed, while thermocline displacements are important in the eastern Pacific on interannual time scales, zonal advection is important in the central Pacific (Picaut et al. 1996). Therefore, it is crucial in order to study the importance of the different oceanic mechanisms at work on ENSO time scales to use a model which performs well in simulating both the sea level and the surface currents. Although long equatorial wave dynamics do not allow one to represent the contributions of non-linear processes and eddies which play an important role in maintaining surface currents (Yu et al. 1997; Yu and McPhaden 1999), a linear model is an interesting tool to investigate the role of long equatorial waves on low-frequency ocean dynamics and thermodynamics. The present study therefore focused on improving the simulation of the long wave component of the surface zonal currents.

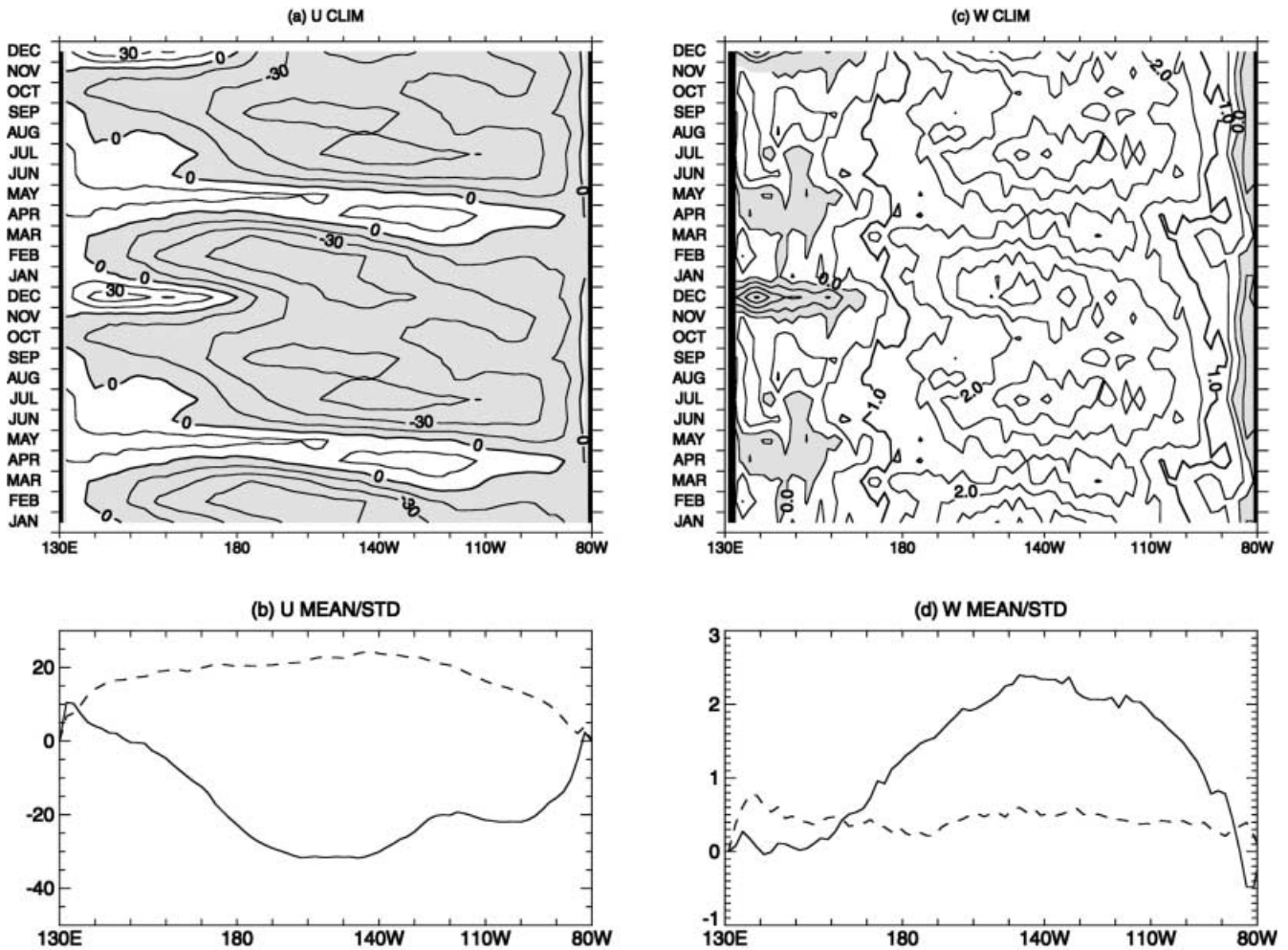


Fig. 7 **a** Longitude–time section plot of the simulated climatological equatorial surface zonal current anomalies (contours are every 15 cm/s and negative values are shaded; three years are presented for clarity); **b** longitude section of the equatorial mean surface zonal current (solid line) and variability (dashed line); **c** longitude–time

section plot of the simulated climatological vertical velocity (contours are every 0.5 m/day and negative values are shaded; three years are presented for clarity); **d** longitude section of the equatorial mean vertical velocity (solid line) and variability (dashed line)

The ocean model presented in that studies the oceanic component of the Trident model (see Boulanger and Menkes 2000 in the same issue which describes the model thermodynamics). Briefly, the ocean dynamics is derived from a linear 3-1/2 layer model with a constant surface layer (mixed-layer). Fluxes of mass and momentum are allowed between the first and second layers. That sets the forcing conditions for the subsurface dynamics. As the surface layer has a constant depth, two baroclinic modes exist in the model.

Two major parameters are investigated to discuss the sensitivity of a linear model in simulating surface zonal currents: the friction formulation and amplitude, and the addition of a second baroclinic mode. Considering the first point, it is shown that the use of weak Rayleigh friction values as used in most of linear models (Zebiak and Cane 1987; Battisti 1988; Picaut et al. 1997) does not allow one to properly simulate the mean state, or the seasonal and interannual variability of the large-scale surface zonal currents. While the addition of a second

baroclinic mode (e.g. Chen et al. 1995; Dewitte 2000) is an improvement (it mainly reduces the simulated large amplitude of westward propagating Rossby waves), the comparisons to observations are still poor in terms of amplitude and variability. When strong Rayleigh friction is used (such as (6 months^{-1}) , the model better simulates the zonal current variability, although it still remains too large.

A new parametrization for the friction was introduced. It consists of a quadratic friction on the momentum equations. The quadratic friction parameter is equivalent to a Rayleigh friction divided by a constant current amplitude. Briefly, this is equivalent to considering a spatially and temporally variable Rayleigh friction: the friction acts more strongly (weakly) when the surface currents are strong (weak), such as in the eastern (western) Pacific and during La Niña (as El Niño) events. The model comparison to the Reverdin et al. (1994) surface current climatology, to the TOPEX/POSEIDON sea level anomalies and to the TAO currents

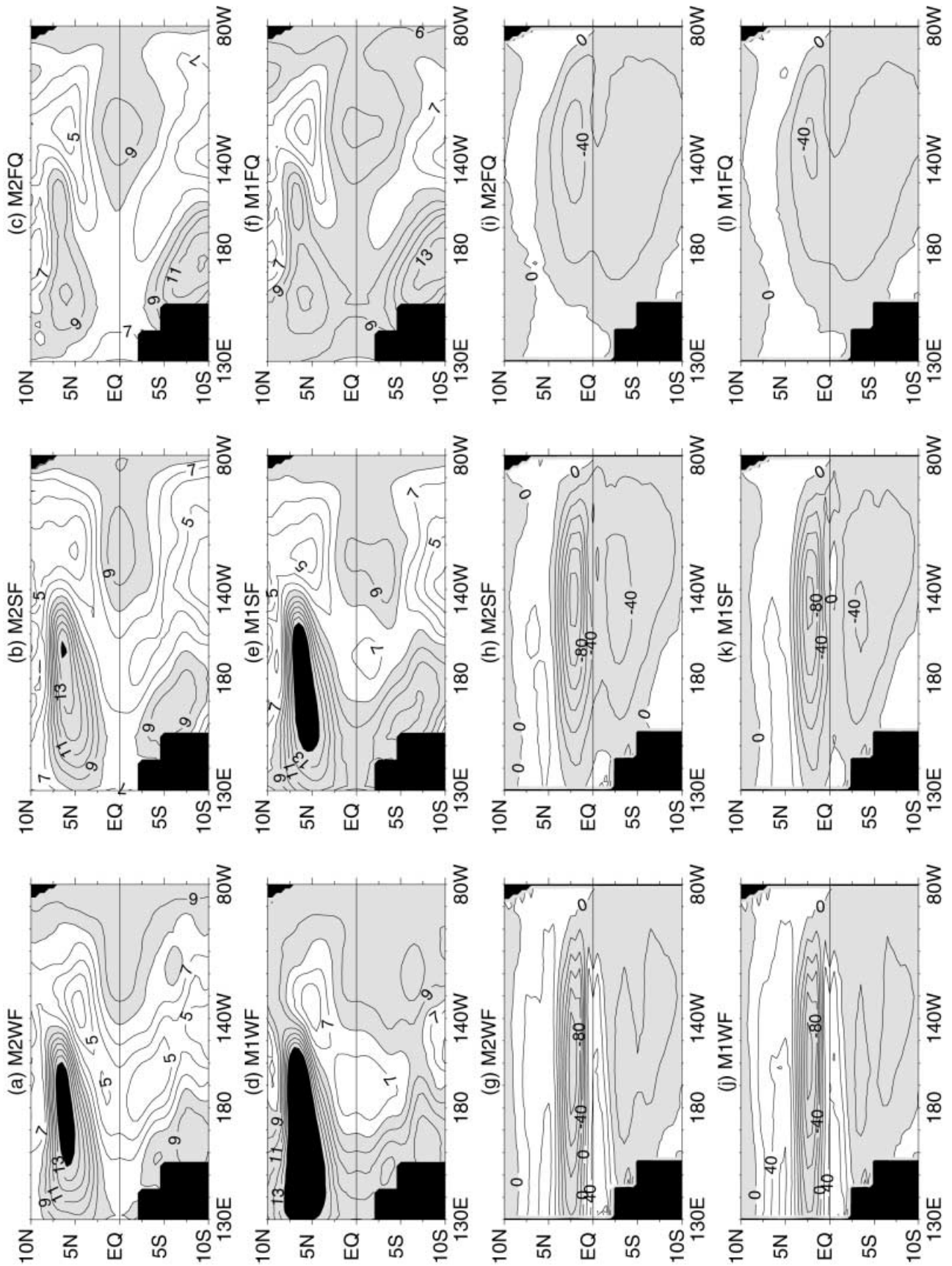


Fig. 8a-f Interannual sea level variability simulated for parameters respectively corresponding to simulations *M2WF*, *M2SF*, *M2FQ*, *M1WF*, *M1SF*, *M1FQ* (contour intervals every 1 cm, values larger than 8 cm are shaded); **g-l** mean zonal currents simulated for

parameters respectively corresponding to simulations *M2WF*, *M2SF*, *M2FQ*, *M1WF*, *M1SF*, *M1FQ* (contour intervals every 20 cm/s, negative values are shaded)

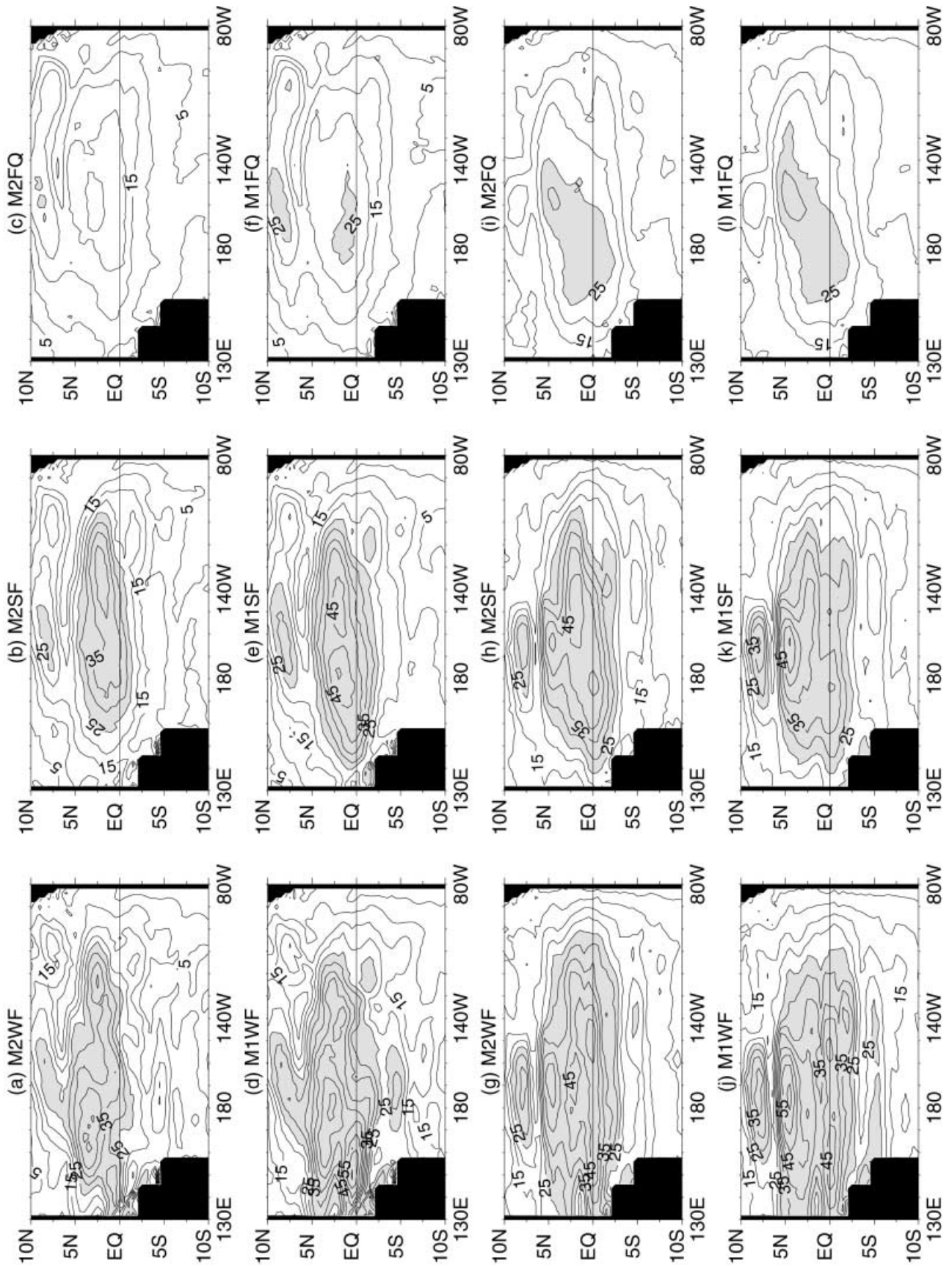


Fig. 9a-f Climatological zonal current variability simulated for parameters respectively corresponding to simulations *M2WF*, *M2SF*, *M2FQ*, *M1WF*, *M1SF*, *M1FQ* (contour intervals every 5 cm/s, values larger than 25 cm/s are shaded); **g-l** interannual zonal

current variability simulated for parameters respectively corresponding to simulations *M2WF*, *M2SF*, *M2FQ*, *M1WF*, *M1SF*, *M1FQ* (contour intervals every 5 cm/s, values larger than 25 cm/s are shaded)

show that it has better skill in simulating sea level and surface current variability. Although the model is less sensitive to the addition of a second baroclinic mode when using quadratic friction, the model currents are improved when two baroclinic modes are considered. The present model used with quadratic friction gives confidence in investigation of the role of long equatorial waves on zonal advection of temperature in relation to ENSO events.

Acknowledgements This research was initiated while at the Jet Propulsion Laboratory, California Institute of Technology, under contract with National Aeronautics and Space Administration. It was completed while working for Centre National de la Recherche Scientifique at Laboratoire d'Océanographie Dynamique et de Climatologie (LODYC, Jussieu, Paris). I am thankful to the Institut National des Sciences de l'Univers (INSU) and the Programme National d'Etude de la Dynamique du Climat (PNEDC) for their financial support. The author wants to thank the Center for Space Research from the University of Texas for providing the processed and gridded TOPEX/POSEIDON data, the Center ERS d'Archivage et de Traitement located in the Institut Français de Recherche pour l'Exploitation de la Mer for providing the processed and gridded ERS-1 and ERS-2 zonal wind stress data, and the PMEL for providing TAO data. I also want to thank Lee-Lueng Fu for his constant support, Claire Perigaud for her useful comments, as well as all the people from the Ocean Science Element at JPL who helped me or with whom I had discussions during my 2-year stay there. I also want to thank Amy Clement, Pascale Delecluse, Eric Guilyardi, Gurvan Madec, Gilles Reverdin, Jérôme Sirven, Jérôme Vialard and many people from LODYC who contributed to the evolution and design of the Trident model. Keith A. Rodgers is greatly thanked for his proof-reading comments which considerably helped in improving the English version of the manuscript. Last but not least, special thanks are addressed to my friend Christophe Menkes whose everlasting support, passionate discussions and Mylodon-like screams helped me complete this long and sometimes excruciating work. Finally, the comments of Mike McPhaden and two other anonymous reviewers considerably helped in improving the scientific content of the present study.

Appendix A

Following the same notations as in McCreary et al. (1992), the subsurface layer equations can be written:

$$\begin{cases} \partial_t \mathbf{u} - \beta y \mathbf{v} + \partial_x (\mathbf{p}/\rho_0) = \mathbf{F} \\ \beta y \mathbf{u} + \partial_y (\mathbf{p}/\rho_0) = \mathbf{G} \\ \mathbf{A} \partial_t (\mathbf{p}/\rho_0) + (\partial_x \mathbf{u} + \partial_y \mathbf{v}) = \mathbf{Q} \end{cases}$$

where the matrix \mathbf{A} relates h and p (with $g_{ij} = g(\rho_j - \rho_i)/\rho_0$) as follows:

$$\mathbf{A} = \begin{pmatrix} 1/(g'_{32}H'_2) & -1/(g'_{32}H'_2) \\ -1/(g'_{32}H'_3) & g'_{42}/(g'_{43}g'_{32}H'_3) \end{pmatrix} = \begin{pmatrix} a_{11} & a_{12} \\ a_{21} & a_{22} \end{pmatrix}$$

and where $\mathbf{q} = \begin{pmatrix} q_2 \\ q_3 \end{pmatrix}$ represents the zonal or meridional current, the pressure anomalies, the zonal or meridional stress or the entrainment velocity in each subsurface layer. The solution to the two layer system can be actually represented as expansions in the two baroclinic (vertical normal) modes: $\mathbf{q} = q_1 \psi_1 + q_2 \psi_2$ where the eigenvectors and eigenvalues of the matrix \mathbf{A} are respectively $\psi_n = \begin{pmatrix} 1 \\ (\lambda_n - a_{11})/a_{12} \end{pmatrix}$ and $\lambda_n = c_n^{-2} = \frac{1}{2}[(a_{11} + a_{22}) + (-1)^n [(a_{11} - a_{22})^2 + 4a_{12}a_{21}]^{1/2}]$. Introducing the eigenvectors $\hat{\psi}_n = \begin{pmatrix} 1 \\ (\lambda_n - a_{11})/a_{21} \end{pmatrix}$ of the adjoint matrix of \mathbf{A} , we can define a scalar

product such that $\langle \mathbf{q} | \psi_n \rangle = q_1 \bar{\psi}_1 \hat{\psi}_n + q_2 \bar{\psi}_2 \hat{\psi}_n$ where $\bar{\psi}_n = (1(\lambda_n - a_{11})/a_{12})$. The norm of the eigenvector n is then $\gamma_n = \langle \psi_n | \psi_n \rangle = \psi_n \hat{\psi}_n = 1 + (\lambda_n - a_{11})^2 / (a_{12}a_{21})$. Thus the system of equations for each baroclinic mode ($j = 1, 2$) is:

$$\begin{cases} \partial_t \mathbf{u}_j - \beta y \mathbf{v}_j + \partial_x (p_j/\rho_0) = F_j \\ \beta y \mathbf{u}_j + \partial_y (p_j/\rho_0) = G_j \\ \partial_t (p_j/\rho_0) + \lambda_j^{-1} (\partial_x \mathbf{u}_j + \partial_y \mathbf{v}_j) = Q_j/\lambda_j \end{cases}$$

with $q_j = \langle \mathbf{q} | \psi_j \rangle / \langle \psi_j | \psi_j \rangle = (q_2 + q_3(\lambda_j - a_{11})/a_{21})/\gamma_j$. Therefore the ratio of upper layer to lower layer variables for each mode j is $r_j = a_{12}/(\lambda_j - a_{11})$.

The solutions of each system of baroclinic equations is then solved using a model similar to Cane and Patton (1984). The major differences from Cane and Patton (1984) is in solving the Kelvin wave equation and in the temporal scheme which is now a leapfrog scheme. The Kelvin wave equation is not solved by integrating the wind forcing, but by solving the discretized Kelvin wave equations from west to east in the same way as the non-Kelvin wave solution. Thus, the scheme is unconditionally stable, and allows us to represent the coastline with a zonal resolution as short as the model zonal grid resolution, whereas in Cane and Patton (1984), it cannot be smaller than the distance that a Kelvin wave travels in one time step.

Finally, at each time step, the horizontal currents and the thickness anomalies of the subsurface layers are then computed from the combination of the baroclinic solutions. It is worth pointing out that when a quadratic friction is used in the layer equations, the two baroclinic solutions are not independent of each other.

References

- Asselin R (1972) Frequency filter for time integrations. *Mon Weather Rev* 100: 487–490
- Battisti DS (1988) Dynamics and thermodynamics of a warming event in a coupled tropical atmosphere-ocean model. *J Atmos Sci* 45: 2889–2819
- Bentamy A, Quilfen Y, Gohin F, Grima N, Lenaour M, Servain J (1996) Determination and validation of average wind fields from ERS-1 scatterometer measurements. *Global Atmos Ocean Syst* 4: 1–29
- Blumenthal MB, Cane MA (1989) Accounting for parameter uncertainties in model verification: an illustration with tropical sea surface temperature. *J Phys Oceanogr* 19: 815–830
- Boullanger J-P, Menkes C (1995) Propagation and reflection of long equatorial waves in the Pacific ocean during the 1992–1993 El Niño. *J Geophys Res* 100: 25 041–25 059
- Boullanger J-P, Fu L-L (1996) Evidence of boundary reflection of Kelvin wave and first-mode Rossby waves from TOPEX/POSEIDON sea level data. *J Geophys Res* 101: 16 361–16 371
- Boullanger J-P, Menkes C (1999) Long equatorial wave reflection in the Pacific Ocean during the 1992–1998 TOPEX/POSEIDON period. *Clim Dyn* 15: 205–225
- Boullanger J-P, Menkes C (2000) The TRIDENT Pacific model. Part II: The thermodynamical model and the role of long equatorial wave reflection during the 1993–1998 TOPEX/POSEIDON period. *Clim Dyn* 17: 175–186
- Bryden HL, Brady EC (1985) Diagnostic model of the three-dimensional circulation in the upper equatorial ocean. *J Phys Oceanogr* 15: 1255–1273
- Busalacchi AJ, O'Brien JJ (1981) Interannual variability of the equatorial Pacific in the 1960s. *J Geophys Res* 86: 10 901–10 907
- Busalacchi AJ, Takeuchi K, O'Brien JJ (1983) Interannual variability of the equatorial Pacific-revisited. *J Geophys Res* 88: 7551–7562
- Busalacchi AJ, Cane MA (1985) Hindcasts of sea level variations during the 1982–1983 El Niño. *J Phys Oceanogr* 15: 213–221

- Busalacchi AJ, McPhaden MJ, Picaut J, Springer SR (1990) Sensitivity of wind-driven tropical Pacific Ocean simulations on seasonal and interannual time scales. *J Mar Sys* 1: 119–154
- Cane MA, Patton RJ (1984) A numerical model for low-frequency equatorial dynamics. *J Phys Oceanogr* 12: 1853–1863
- Cane MA, Sarachik E (1979) Forced baroclinic ocean motions. III: the linear equatorial basin case. *J Mar Res* 37: 355–398
- Cane MA, Sarachik E (1977) Forced baroclinic ocean motions. II: the linear equatorial bounded case. *J Mar Res* 35: 395–432
- Cane MA, Sarachik E (1976) Forced baroclinic ocean motions. I: the linear equatorial unbounded case. *J Mar Res* 34: 629–665
- Chen D, Rothstein LM, Busalacchi AJ (1994) A hybrid vertical mixing scheme and its application to tropical ocean models. *J Phys Oceanogr* 24: 2156–2179
- Chen Y-Q, Battisti DS, Sarachik ES (1995) A new ocean model for studying the tropical oceanic aspects of ENSO. *J Phys Oceanogr* 25: 2065–2089
- Cromwell T (1953) Circulation in a meridional plane in the central equatorial Pacific. *J Mar Res* 12: 196–213
- Delcroix T, Boulanger J-P, Masia F, Menkes C (1994) GEOSAT-derived sea level and surface-current anomalies in the equatorial Pacific, during the 1986–1989 El Niño and La Niña. *J Geophys Res* 99: 25 093–25 107
- Delcroix T, Picaut J, Eldin G (1991) Equatorial Kelvin and Rossby waves evidenced in the Pacific Ocean through GEOSAT sea level and surface currents. *J Geophys Res* 96: 3249–3262
- Dewitte B (2000) Sensitivity of an intermediate ocean-atmosphere coupled model of the Tropical Pacific to its oceanic structure. *J Clim* 29: 1542–1570
- Halpern D (1987) Observations of annual and El Niño thermal and flow variations at 0°, 110°W and 0°, 95°W during 1980–1985. *J Geophys Res* 92: 7289–7312
- Hayes SP, Mangum LJ, Picaut J, Sumi A, Takeuchi K (1991) TOGA-TAO: a moored array for real-time measurements in the tropical Pacific ocean. *Bull Am Meteorol Soc* 72: 3339–3347
- Kessler WS, McPhaden MJ (1995) Oceanic equatorial waves and the 1991–1993 El Niño. *J Clim* 8: 1757–1774
- McCreary J (1985) Modelling equatorial oceanic circulation. *Annu Rev Fluid Mech* 17: 359–409
- McCreary J, Fukamachi Y, Lu P (1992) A non-linear mechanism for maintaining coastally trapped eastern boundary currents. *J Geophys Res* 97: 5677–5692
- McPhaden MJ (1993) TOGA-TAO and the 1991–93 El Niño–Southern Oscillation event. *Oceanography* 6: 36–44
- McPhaden MJ, Hayes SP (1990) Moored velocity, temperature and wind measurements in the equatorial Pacific Ocean: a review of scientific results, 1985–1990. *Intl TOGA Sci Conf Proc*, Geneva, Switzerland, World Meteorological Organization, pp 59–69
- McPhaden MJ, McCarthy ME (1992) Mean seasonal cycles and interannual variations at 0°, 110°W and 0°, 140°W during 1980–1991. *NOAA Tech Mem ERL PMEL-95*, pp 118
- McPhaden MJ, Yu X (2000) Equatorial waves and the 1997–1998 El Niño. *Geophys Res Lett* (in press)
- Menkes C, Boulanger J-P, Busalacchi AJ, Vialard J, Delecluse P, McPhaden MJ, Hackert E, Grima N (1998) Impact of TAO versus ERS wind stresses onto simulations of the tropical Pacific Ocean during the 1993–1998 period by the OPA OGCM. In: *Climatic impact of scale interactions for the tropical ocean-atmosphere system*, pp 46–48, Euroclivar Workshop Report, Eucliv 13
- Miller L, Cheney R, Douglas B (1988) GEOSAT altimeter observations of Kelvin waves and the 1986–1987 El Niño. *Science* 239: 52–54
- Moore DW, Philander SGH (1977) Modelling of the tropical oceanic circulation. In: *Glodberg ED, McCave IN, O'Brien JJ, Steele JH (eds) The sea*, vol. 6, John Wiley and Sons, Chichester, pp 319–361
- Picaut J, Masia F, duPenhoat Y (1997) An advective-reflective conceptual model for the oscillatory nature of the ENSO. *Science* 277: 663–666
- Picaut J, Ioualalen M, Menkes C, Delcroix T, McPhaden MJ (1996) Mechanism of the zonal displacements of the Pacific warm pool: implications for ENSO. *Science* 274: 1486–1489
- Picaut J, Delcroix T (1995) Equatorial wave sequence associated with warm pool displacements during the 1986–1989 El Niño–La Niña. *J Geophys Res* 100: 18 393–18 408
- Picaut J, Menkes C, Boulanger J-P, duPenhoat Y (1993) Dissipation in a Pacific equatorial long wave model. In: *TOGA-Notes*, 10, Nova University Press, Dania FL, pp 11–15
- Reverdin G, Frankignoul C, Kastenare E, McPhaden MJ (1994) Seasonal variability in the surface currents of the equatorial Pacific. *J Geophys Res* 99: 20 323–20 344
- Schopf PS, Suarez MJ (1988) Vacillations in a coupled ocean-atmosphere model. *J Atmos Sci* 45: 549–566
- Tapley BD, Chambers DP, Shum CK, Eanes RJ, Ries JC (1994) Accuracy assessment of the large-scale dynamic ocean topography from TOPEX/POSEIDON altimetry. *J Geophys Res* 99: 24 605–24 617
- Vialard J, Menkes C, Boulanger J-P, Delecluse P, Guilyardi E, McPhaden MJ (2000) Oceanic mechanisms driving the SST during the 1997–1998 El Niño. *J Phys Oceanogr* (in press)
- Wang W, McPhaden MJ (1999) The surface layer heat balance in the equatorial Pacific ocean, part I: mean seasonal cycle. *J Phys Oceanogr* 29: 1812–1831
- Wang W, McPhaden MJ (2000) The surface layer heat balance in the equatorial Pacific ocean, Part II: interannual variability. *J Phys Oceanogr* (in press)
- Yu X, McPhaden MJ (1999) Seasonal variability in the equatorial Pacific. *J Phys Oceanogr* 29: 925–947
- Yu Z, Schopf PS, McCreary JP (1997) On the annual cycle of upper ocean circulation in the eastern equatorial Pacific. *J Phys Oceanogr* 27: 309–324
- Zebiak SE, Cane MA (1987) A model El Niño/Southern Oscillation. *Mon Weather Rev* 115: 2262–2278